The effect of gravity on liquid plug propagation in a two-dimensional channel

V. Suresh and J. B. Grotberg[a)]
Department of Biomedical Engineering, University of Michigan, Ann Arbor, Michigan 48109

(Received 21 May 2004; accepted 5 October 2004; published online 1 March 2005)

The effect of plug propagation speed and gravity on the quasisteady motion of a liquid plug in a two-dimensional liquid-lined channel oriented at an angle α with respect to gravity is studied. The problem is motivated by the transport of liquid plugs instilled into pulmonary airways in medical treatments such as surfactant replacement therapy, drug delivery, and liquid ventilation. The capillary number Ca is assumed to be small, while the Bond number Bo is arbitrary. Using matched asymptotic expansions and lubrication theory, expressions are obtained for the thickness of the trailing films left behind by the plug and the pressure drop across it as functions of Ca, Bo, α and the thickness of the precursor films. When the Bond number is small it is found that the trailing film thickness and the flow contribution to the pressure drop scale as $Ca^{2/3}$ at leading order with coefficients that depend on Bo and α. The first correction to the film thickness is found to occur at $O(Ca)$ compared to $O(Ca^{4/3})$ in the $Bo=0$ case. Asymmetry in the liquid distribution is quantified by calculating the ratio of liquid volumes above and below the centerline of the channel, V_R. $V_R=1$ at $Bo=0$, indicating a symmetric distribution, and decreases with Bo and Ca, but increases with the plug length L_p. The decrease of V_R with Ca suggests that higher propagation speeds in small airways may result in less homogenous liquid distribution, which is in contrast to the expected effect in large airways. For given values of the other parameters, a maximum capillary number Ca_c is identified above which the plug will eventually rupture. When the Bond number becomes equal to an orientation-dependent critical value Bo_c, it is found that the scaling of the film thickness and pressure drop change to $Ca^{1/2}$ and $Ca^{1/6}$, respectively. It is shown that this scaling is valid for small increments of the Bond number over its critical value, $Bo=Bo_c+BCa^{1/6}$, but for higher Bond numbers the asymptotic approach breaks down. © *2005 American Institute of Physics*.
[DOI: 10.1063/1.1863853]

I. INTRODUCTION

Liquid is instilled into the lungs during medical treatments such as surfactant replacement therapy (SRT),[1–3] partial liquid ventilation (PLV),[4–7] and pulmonary drug/genetic material delivery.[8–13] The instilled liquid may form a meniscus in the trachea[14] and be transported through the airways in the form of air-blown plugs; it may also drain gravitationally through the larger airways and form plugs in the smaller airways.[15] The effectiveness of the treatment can depend on: (1) delivery to the desired location via liquid deposition in films left behind by propagating plugs and (2) the homogeneous distribution of liquid through the branching airway network as plugs split at airway bifurcations. In turn, these factors are influenced by a number of parameters including liquid and interfacial properties, propagation speed, gravity, and airway orientation.[15–17] An understanding of the fluid dynamics of plug propagation would therefore be useful in devising strategies to ensure optimal liquid distribution in the lung.

In this paper we focus on the effect of gravitational acceleration g on plug propagation. Gravitational effects can be important since the Bond number $Bo=\rho g a^2/\sigma$, based on the airway radius a, liquid density ρ, and surface tension at the air-liquid interface σ, can vary in the range 10^{-4}–10^2 in typical clinical situations.[18] In addition, airway orientation with respect to gravity must also be considered since the human airway network has a three-dimensional branching structure.[19] Consider a plug that moves through a liquid-lined airway oriented at an angle α to gravity and splits at an airway bifurcation as shown in Fig. 1. Gravity affects the volume of liquid delivered to each downstream branch in two ways. First, less liquid enters the upper branch since work needs to be done against gravity. Second, gravity causes a larger fraction of the plug to be present *below* the centerline of the parent airway prior to the bifurcation compared to *above*, and this asymmetry predisposes a larger fraction of the plug volume to enter the lower branch. This unequal splitting is repeated at each subsequent bifurcation, leading to an overall nonhomogeneous liquid distribution in the lung. One of the aims of this work is to quantify the plug's prebifurcation asymmetry in the liquid distribution and determine its dependence on various parameters.

Gravity and airway orientation also affect the thickness of the films deposited by the plug, which ultimately influences liquid distribution. If the films are thick, the plug loses volume more rapidly and may rupture before it reaches the intended delivery site. On the other hand, if plugs persist over an entire cycle of breathing or are created prior to ex-

[a)]Author to whom correspondence should be addressed.

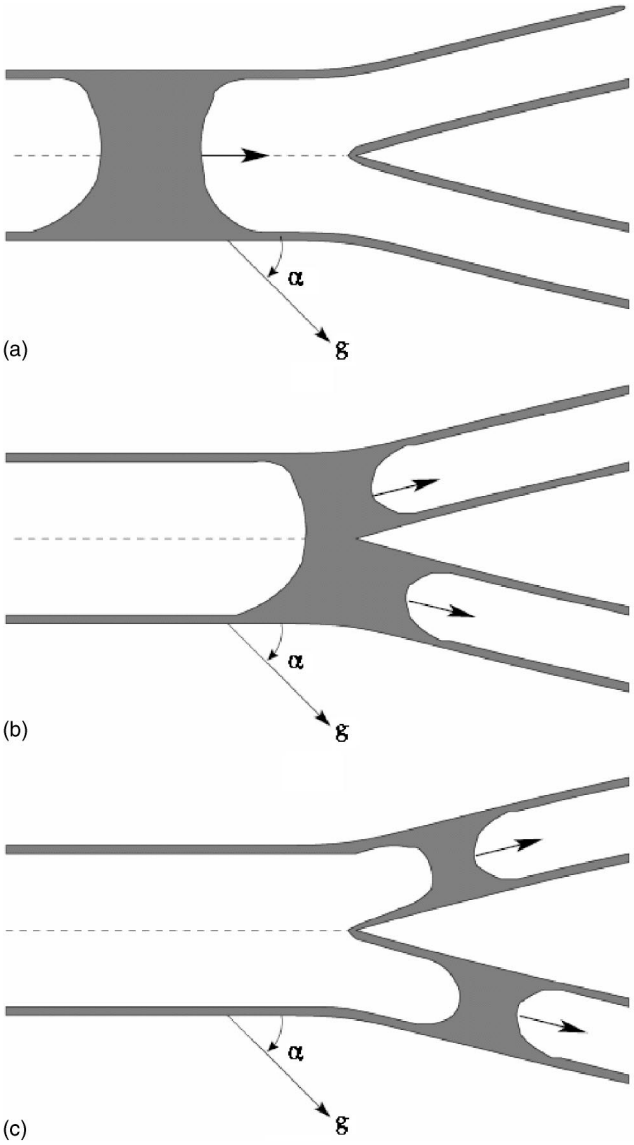

FIG. 1. Schematic of plug motion through an airway bifurcation. (a) A liquid plug moves through a liquid lined airway. The plug volume is asymmetrically distributed about the centerline of the airway due to gravity. (b) The plug enters an airway bifurcation and (c) subsequently splits into two with a larger fraction of the original plug entering the lower, gravity-favored branch.

piration, liquid may be blown out of the lung during exhalation. Therefore, a second aim of this work is to determine how gravity and airway orientation affect the possibility of plug rupture.

In the smaller distal airways, the plug propagation speed $\bar{U}$ is typically slow and the capillary number $Ca=\mu\bar{U}/\sigma$, where μ is the liquid viscosity, is small. The problem of plug propagation in a cylindrical geometry in the presence of gravity is highly complicated due to the lack of azimuthal symmetry. In order to simplify the analysis we study the low capillary number, pressure driven motion of a liquid plug through a two-dimensional channel oriented at an angle α with respect to gravity. This simplification neglects the destabilizing radial component of interfacial curvature that is responsible for a Rayleigh instability of the liquid film that can lead to the formation of liquid plugs in airways. The focus of this work is on preexisting plugs that are either introduced into airways during a medical procedure or form due to instabilities. In particular, the prebifurcation asymmetry and liquid deposition depend on the effect of gravity on the longitudinal curvature of the interface, which is retained in the two-dimensional model.

An analysis of the low capillary number motion of a long bubble through a tube was carried out by Bretherton[20] who found that the thickness of the liquid film separating the bubble and the tube wall and the pressure drop across the bubble both scaled as $Ca^{2/3}$. His work was formalized in the terminology of matched asymptotic expansions by Park and Homsy.[21] Other authors have examined flow in polygonal capillaries,[22,23] surfactant effects[24–28] and thermocapillary migration.[29,30] In the context of airway plug propagation, small capillary number asymptotic theory has been used to study problems in airway reopening in rigid[31] and flexible[32,33] channels and tubes and surfactant effects on plug propagation.[34] None of these studies considered the effects of gravity.

Jensen *et al.*[35] examined the effect of gravity on the displacement of liquid by an air finger in a horizontal Hele–Shaw cell using theory and experiment. For $Bo<1$ they found that the film thickness followed the $Ca^{2/3}$ scaling of Bretherton with *Bo* dependent coefficients, while the pressure jump across the air-liquid interface was independent of *Bo*. For $Bo\geqslant 1$ the lower film was an $O(1)$ quantity independent of *Ca*. Both the film thickness and pressure jump increased with *Bo*. The experimentally observed meniscus shapes were in agreement with the theory. Lasseux and Quintard[36] and Lasseux[37] studied gravitational gas-liquid drainage in vertical Hele–Shaw cells and capillary tubes and also found that the Bretherton scaling applies with *Bo* dependent coefficients.

Plug propagation in a tube or channel is closely related to coating flow, a classical example of which is the withdrawal of a fiber or plate from a liquid bath. The review by Quéré[38] provides an excellent overview of existing literature. Early work found the film thickness to scale as $Ca^{2/3}$ when gravitational drainage in the entrained film was neglected.[39,40] These results were recast in the form of matched asymptotic expansions by Wilson[41] and extended to account for nonvertical withdrawal. In the gravity dominated case a thickness proportional to $Ca^{1/2}$ was predicted.[42] Approximations for the crossover between the two regimes showed reasonable agreement with experiment.[43,44]

The small *Ca* asymptotic analysis of gas-liquid displacement and coating flows shows that the same scaling laws arise in both situations: When gravitational effects are small a static meniscus is connected to a thin film of thickness $t\sim Ca^{2/3}$ by a dynamic meniscus of length $l\sim Ca^{1/3}$. When gravitational effects are strong, crossover to a different scaling regime with $t\sim Ca^{1/2}$ occurs in coating flows. In this paper we show that a similar crossover occurs when *Bo* is increased for plug propagation in an inclined channel. The paper is organized as follows. In Sec. II we describe the model and discuss the basic equations and scaling arguments in different regimes. In Secs. III and IV we provide a systematic development of the asymptotic equations and their

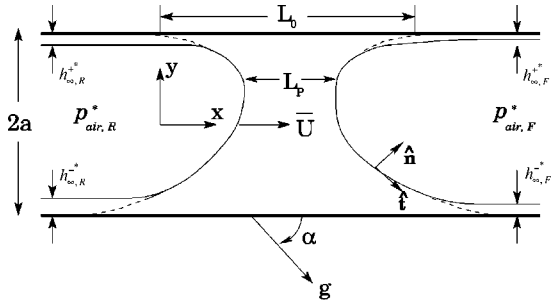

FIG. 2. Schematic of the model showing the propagating plug and thin films. The dashed lines represent the static solutions for the rear and front interfaces, and $x=0$ is located at the intersection of the static rear interface with the upper wall. L_0 is the distance between the contact points of the rear and front static solutions with the upper wall. L_p is the length of the plug and is equal to the distance between the tips of the two interfaces. L_0 and L_p are not independent parameters, see Sec. III A for explanation.

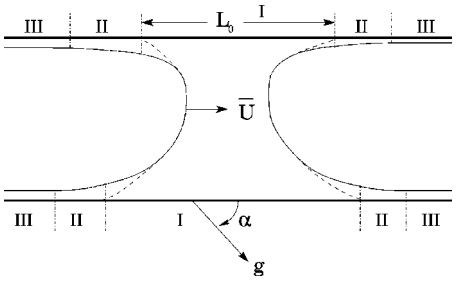

FIG. 3. Schematic showing (I) the statics region close to the body of the plug; (II) four transition regions close to the upper and lower walls at the front and rear meniscus; and (III) trailing and precursor thin films.

solutions. We conclude in Sec. V with a discussion of the results and their applicability to human airways.

II. FORMULATION

A. Model description

A schematic of the model is shown in Fig. 2. It consists of a plug of incompressible, Newtonian fluid of viscosity μ and density ρ moving at constant speed $\bar{U}$ in the laboratory frame through a two-dimensional channel of thickness $2a$. The channel is oriented at an angle α with respect to the gravitational acceleration g and lined with thin precursor films of the plug fluid. The plug separates two semiinfinite air fingers of negligible viscosity and density. The surface tension at the air-liquid interface is assumed to be constant and equal to σ.

Dimensional variables are denoted by superscript *. We use a Cartesian coordinate system (x^*,y^*) with the channel walls located at $y^*=\pm a$ and seek a steady solution in the frame of the moving plug. Fluid velocity and pressure in the plug fluid are denoted by $\mathbf{u}^*=(u^*,v^*)$ and p^* respectively. Air pressures behind and ahead of the plug are constant and equal to $p^*_{air,R}$ and $p^*_{air,F}$. The air-liquid interface is located at $y^*=h^{\pm^*}(x^*)$. Superscript $^+$ and $^-$ denote quantities in the upper and lower parts of the channel, respectively. As the plug moves through the channel, it deposits trailing films on the upper and lower walls, whose thicknesses $h^{+^*}_{\infty,R}$ and $h^{-^*}_{\infty,R}$ will be determined. The corresponding precursor film thicknesses ahead of the plug are specified and equal to $h^{+^*}_{\infty,F}$ and $h^{-^*}_{\infty,F}$. Subscript "*R*" and "*F*" denote quantities behind (rear) and ahead (front) of the plug, and will be dropped when an expression applies both ahead and behind the plug.

B. Dimensionless groups and governing equations

Lengths are scaled by the channel half-width a, velocities by the propagation speed $\bar{U}$, and pressures by the capillary scale σ/a. We assume that the plug motion is sufficiently slow that inertial effects can be neglected and set the Reynolds number $Re=\rho\bar{U}a/\mu$ equal to zero. Then the relevant dimensionless groups are the capillary number $Ca=\mu\bar{U}/\sigma$ and the Bond number $Bo=\rho g a^2/\sigma$. Dropping the superscript *, the dimensionless steady Stokes and continuity equations are

$$-\nabla p + Ca\nabla^2\mathbf{u} + Bo\hat{\mathbf{g}} = 0, \tag{1}$$

$$\nabla\cdot\mathbf{u} = \mathbf{0}, \tag{2}$$

where $\hat{\mathbf{g}}=[\cos(\alpha),-\sin(\alpha)]$ is the unit vector in the direction of gravity. The boundary conditions are

$$u=-1, v=0 \text{ at } y=\pm 1, \tag{3}$$

$$\mathbf{u}\cdot\hat{\mathbf{n}} = 0 \text{ at } y=h^{\pm}(x), \tag{4}$$

$$\hat{\mathbf{t}}\cdot\boldsymbol{\sigma}\cdot\hat{\mathbf{n}} = 0 \text{ at } y=h^{\pm}(x), \tag{5}$$

$$p-p_{air}-\hat{\mathbf{n}}\cdot\boldsymbol{\sigma}\cdot\hat{\mathbf{n}} = \nabla\cdot\hat{\mathbf{n}} \text{ at } y=h^{\pm}(x). \tag{6}$$

These represent, respectively, no-slip and no penetration at the channel walls, and the kinematic condition, shear, and normal stress balances at the air-liquid interface, $y=h^{\pm}(x)$. Here $\boldsymbol{\sigma}=Ca(\nabla\mathbf{u}+\nabla\mathbf{u}^T)$ is the fluid extra stress tensor, $\hat{\mathbf{n}}$ is the outward pointing unit normal, $\hat{\mathbf{t}}$ is the tangent to the interface, and $\nabla\cdot\hat{\mathbf{n}}$ is the interfacial curvature.

C. Asymptotic scaling and regimes

We seek an asymptotic solution of the governing equations in the limit $Ca\to 0$. The analysis closely follows that of previous works.[21,32,34,35] For small Ca the flow domain can be divided into three regions as shown in Fig. 3: (I) a statics region close to the body of the plug in which surface tension and gravitational body forces are important, but viscous forces are negligible; (II) thin transition regions close to the walls in which viscous, surface tension, and gravitational body forces are important; and (III) flat thin films away from the plug.

Two different force balances are possible in the transition regions, which lead to different scalings for the film thickness as explained below. Suppose that the transition region is a thin layer of length l and thickness t, such that t

$\ll a$. Then the interfacial curvature in the transition region is $\kappa_{tr} \sim t/l^2$ leading to a surface tension pressure scale

$$p_{cap} \sim \sigma \kappa_{tr} \sim \sigma t/l^2. \tag{7}$$

The viscous pressure scale in the transition region is

$$p_{vis} \sim \mu U l/t^2. \tag{8}$$

First consider the case $g=0$ In the absence of gravity, the viscous and surface tension pressure scales must balance and setting $p_{cap}=p_{vis}$ leads to

$$t/l \sim Ca^{1/3}. \tag{9}$$

κ_{tr} must match the curvature of the meniscus in the statics region, $\kappa_{st} \sim 1/a$, when these regions overlap and so equating the two curvatures results in

$$t/l^2 \sim 1/a. \tag{10}$$

Equations (7)–(10) lead to the scalings[20,21,32,34]

$$l/a \sim Ca^{1/3},$$

$$t/a \sim Ca^{2/3},$$

$$p_{tr}/(\sigma/a) \sim 1, \tag{11}$$

where $p_{tr} \sim p_{vis} \sim p_{st}$ is the pressure scale in the transition region. We call this the *viscocapillary regime* based on the dominant forces in the transition region.

When $g \neq 0$ there is also a hydrostatic pressure scale based on the length of the transition region,

$$p_g = \rho g l \cos(\alpha), \tag{12}$$

and κ_{st} is affected by gravity, i.e., $\kappa_{st}=\kappa_{st}(Bo, \alpha)$. However, the viscocapillary scaling (11) is valid if the following two conditions are satisfied: (i) the dominant balance in the transition region is between the viscous and surface tension terms [Eq. (9) is valid] and gravitational effects are small compared to these terms, i.e.,

$$\frac{p_g}{p_{vis}} \sim \frac{p_g}{p_{cap}} \sim Ca^{1/3} Bo \cos(\alpha) \ll 1, \tag{13}$$

and (ii) $\kappa_{st}(Bo, \alpha)$ remains $O(1/a)$, i.e., (10) holds. These conditions determine constraints on Bo and α for which the asymptotic analysis is valid and we will show later that the restriction on $\kappa_{st}(Bo, \alpha)$ is more critical. For $\alpha=\pi/2$ Jensen *et al.*[35] found that the conditions are satisfied when $Bo<1$, $Ca \ll 1$.

When p_g is the same size as p_{vis} and p_{cap} and $Bo \cos(\alpha)=O(1)$ a different scaling is obtained by equating (7), (8), and (12),

$$l/a \sim Ca^{1/6},$$

$$t/a \sim Ca^{1/2},$$

$$p_{tr}/(\sigma/a) \sim Ca^{1/6}. \tag{14}$$

We call this the *gravitational regime* to emphasize the role of gravity in determining the scaling. In this case the curvature in the overlap region is small, $\kappa_{st} \sim t/l^2 \sim Ca^{1/6}/a \ll 1/a$. Also the film thickness t and transition region length l are larger and p_{tr} smaller by $O(Ca^{1/6})$ compared to the viscocapillary scaling, (11). We will show in the following sections that the viscocapillary scaling holds for small Bo and that for each orientation α, there is a critical Bo at which the scaling changes to (14). Note that $t \ll l$ for both scalings, and so the hydrostatic variation of pressure over the depth of the transition region can be neglected.

D. Perturbation expansion

Velocities, pressures, interface position, and film thickness are written in terms of a perturbation expansion for small Ca. From the preceding analysis a natural choice for the expansion parameter is Ca^a with $a=1/3$ for the viscocapillary regime and $a=1/6$ for the gravitational regime. Thus

$$f = f_0 + Ca^a f_1 + Ca^{2a} f_2 + \cdots, \tag{15}$$

where f can be u, v, p, h, or t. In the transition regions, rescaled variables are defined as

$$X = \frac{x - x_0^{\pm}}{Ca^a},\ Y = \frac{1 \mp y}{Ca^b},\ H^{\pm} = \frac{1 \mp h^{\pm}}{Ca^b},\ T^{\pm} = \frac{h_{\infty}^{\pm}}{Ca^b},$$

$$(U, V) = \left(u, \frac{v}{Ca^{b-a}}\right),\ P = \frac{p}{Ca^c}, \tag{16}$$

where $b=2/3$, $c=0$ for the viscocapillary regime and $b=1/2$, $c=1/6$ for the gravitational regime. The upper (lower) sign in $\pm$, $\mp$ refers to the upper (lower) transition regions. The origins of the transition regions are located at $(x_0^{\pm}, \pm 1)$ and the interface is located at $Y=H^{\pm}(X)$. The velocity scaling follows from the continuity equation (2) and the no-slip boundary condition (3). U, V, P, $H^{\pm}$, and $T^{\pm}$ are also expanded in a perturbation series of the form (15).

E. Matching conditions

The transition regions must be matched to the statics region and the thin films at either end. The matching to the thin films requires that the transition region thickness equal the film thickness far from the plug, i.e., $H^{\pm}(X) \to T^{\pm}$, $X \to \mp\infty$. The limits $-\infty$ and $+\infty$ are valid in the rear and front transition regions, respectively. At the other end, the transition regions overlap with the statics region as $X \to \pm\infty$ and $x \to x_0^{\pm}$. Therefore, the matching criterion is obtained from (16) to be

$$\lim_{x \to x_0^{\pm}} h^{\pm}(x) = \lim_{X \to \begin{cases} +\infty & \text{(rear)} \\ -\infty & \text{(front)} \end{cases}} \pm \left(1 - Ca^b H^{\pm}(X)\right). \tag{17}$$

As described by Park and Homsy,[21] matching conditions at each order are found by expanding $h^{\pm}(x)$ in a Taylor series about $x=x_0^{\pm}$, rewriting in terms of the transition region variables and comparing term by term with the right-hand side of (17).

III. THE VISCOCAPILLARY REGIME

A. $O(Ca^0)$ equations in the statics region

Viscous terms are negligible in (1) up to $O(Ca)$, and the pressure is hydrostatic at leading order,

$$p_0(x,y) = Box\cos(\alpha) - Boy\sin(\alpha) + c_0. \tag{18}$$

The normal stress boundary condition (6) takes the form

$$Box\cos(\alpha) - Boh_0^{\pm}(x)\sin(\alpha) - \delta p_0 = \pm \frac{h_{0,xx}^{\pm}}{(1+h_{0,x}^{\pm 2})^{3/2}}, \tag{19}$$

where $\delta p_0 = \delta p_{0,R} = p_{air,R} - c_0$ for the rear meniscus and $\delta p_0 = \delta p_{0,F} = p_{air,F} - c_0$ for the front meniscus. Thus (19) provides differential equations to determine the shape of the two menisci. A Taylor series expansion of $h_0^{\pm}(x)$ up to $O(Ca^{1/3})$ in (17) gives the boundary conditions

$$h_0^{\pm}(x_0^{\pm}) = \pm 1, \tag{20}$$

$$h_{0,x}^{\pm}(x_0^{\pm}) = 0. \tag{21}$$

In addition, $h_0^+(x)$ and $h_0^-(x)$ must join smoothly at the "tip" of the meniscus, $x = x_t$, where their derivatives are unbounded, i.e.,

$$h_0^+ = h_0^-, \quad h_{0,x}^{\pm} \to \mp\infty \; x = x_t. \tag{22}$$

Equation (22) applies at all orders in Ca. For the rear interface, the origin of the coordinate system is specified by choosing $x_{0,R}^+ = 0$. Specifying L_0 then fixes $x_{0,F}^+$ for the front interface (see Fig. 2). For each interface, the four constraints (20) and (21) along with the smoothness condition (22) specify boundary conditions for (19) and determine δp_0 and x_0^-. Equations (20) and (21) state that the static solution at $O(Ca^0)$ apparently meets the channel walls with a zero contact angle. For any given L_0, the plug length L_P can be determined after solving for the static interfaces. The difference in air pressures between the rear and front of the plug $\Delta p_0 = p_{air,R} - p_{air,F} = \delta p_{0,R} - \delta p_{0,F}$ depends on L_0 (equivalently, the plug length L_P) and counteracts the gravitational body force acting on the plug, preventing it from accelerating.

It can be shown that the front interface satisfies the same equations and boundary conditions as the rear interface when $(x, \alpha, \delta p_{0,F})$ are replaced by $[L_0 - x, \pi - \alpha, \delta p_{0,R} + L_0\cos(\alpha)]$. Therefore, if the solution for the rear interface $y = h_{0,R}^{\pm}(x)$ and the pressure jump $\delta p_{0,R}$ are known for some (Bo, α) and L_0 is specified, the solution for the front interface $y = h_{0,F}^{\pm}(x)$ and the pressure jump $\delta p_{0,F}$ are known for $(Bo, \pi - \alpha)$. In contrast to the $Bo = 0$ case, (19)–(21) do not admit an analytical solution. The system is transformed to arc-length coordinates as described in the Appendix and integrated numerically using the boundary value solver COLMOD which is available for download from the internet at http://www.netlib.org.[45,46]

B. $O(Ca^0)$ equations in the transition regions

To derive the transition region equations, the rescaled variables (16) and the perturbation expansion (15) are substituted into (1)–(6). The momentum and continuity equations reduce to the lubrication equations. Using the lubrication velocity field in the kinematic and normal stress conditions results in a third-order ordinary differential equation for the interface location. The details of the derivation have been discussed by previous authors,[20,21] and carry through with minor modifications when gravity is included. Therefore, we do not repeat the details here and only present the final result that the interface shape is given by the Landau–Levich equation

$$J_{0,\xi\xi\xi}^{\pm} = \frac{3(J_0^{\pm} - 1)}{(J_0^{\pm})^3}, \tag{23}$$

where

$$J_0^{\pm} = H_0^{\pm}/T_0^{\pm}, \; \xi = (X + X_0^{\pm})/T_0^{\pm}. \tag{24}$$

Here $X_0^{\pm}$ is an arbitrary translation of the coordinates, which will be determined by matching to the statics region. Appropriate initial conditions for integrating (23) are obtained from the asymptotic behavior of $J_0^{\pm}$ in the limit $\xi \to -\infty$ in the rear and $\xi \to +\infty$ in the front, where the interface must match the constant film thickness. The initial conditions are of the form

$$J_0^{\pm} \sim 1 + \exp(\lambda\xi), \quad \xi \to -\infty(\text{rear}),$$

$$J_0^{\pm} \sim 1 + A\exp(-\lambda\xi/2)\cos(\sqrt{3}\lambda\xi/2), \quad \xi \to +\infty(\text{front}), \tag{25}$$

where $\lambda = 3^{1/3}$ and A is a free parameter that depends on the precursor film thickness as explained below.

Numerical integration of (23) shows that the asymptotic form of $J_0^{\pm}$ close to the statics region is

$$J_0^{\pm} \sim (A_0^{\pm}/2)\xi^2 + A_1^{\pm}\xi + A_2^{\pm}, \quad \xi \to \pm\infty. \tag{26}$$

Applying the matching condition (17) at $O(Ca^{2/3})$ the film thickness T_0^+ and T_0^- on the upper and lower walls, respectively, are found to be

$$T_0^{\pm} = \frac{A_0^{\pm}}{h_{0,xx}^{\pm}(x_0^{\pm})}. \tag{27}$$

For the trailing films the integration gives $A_0^{\pm} = 1.3375$. Note that $\pm h_{0,xx}^{\pm}(x_0^{\pm})$ is the curvature at $x_0^{\pm}$ since $h_{0,x}^{\pm}(x_0^{\pm}) = 0$, and thus the film thickness is inversely proportional to the local curvature of the statics solution. When $Bo = 0$, it is easy to show that $h_{0,xx}^{\pm}(x_0^{\pm}) = \mp 1$ and (27) reduces to the well-known result of Bretherton.[20] Results for $Bo \geqslant 0$ and different α are plotted in Figs. 4(a) and 4(b). On the lower wall, $T_{0,R}^-$ decreases with increasing Bo for $\alpha = 0$ and passes through a slight maximum for $\alpha = \pi/4$. For $\alpha \geqslant \pi/2$, $T_{0,R}^-$ increases monotonically with Bo and diverges at a finite critical value $Bo = Bo_c$ when $h_{0,xx}^-(x_0^-)$ becomes equal to zero. The upper film is thinner than the lower film ($T_{0,R}^+ < T_{0,R}^-$), except for $\alpha = 0$ and π when $T_{0,R}^+ = T_{0,R}^-$ due to symmetry. $T_{0,R}^+$, in general, decreases with Bo and does not diverge except for $\alpha = \pi$. These results can be summarized as follows: For $\alpha < \pi/2$, viscocapillary solutions can be found for the rear transition regions in which the film thickness on either wall is finite. For $\alpha \geqslant \pi/2$, viscocapillary solutions only exist for Bond numbers less than a critical value Bo_c at which the film thickness on the upper/lower walls diverges. This critical value marks the transition to the gravitational regime, which is discussed in greater detail in Sec. IV.

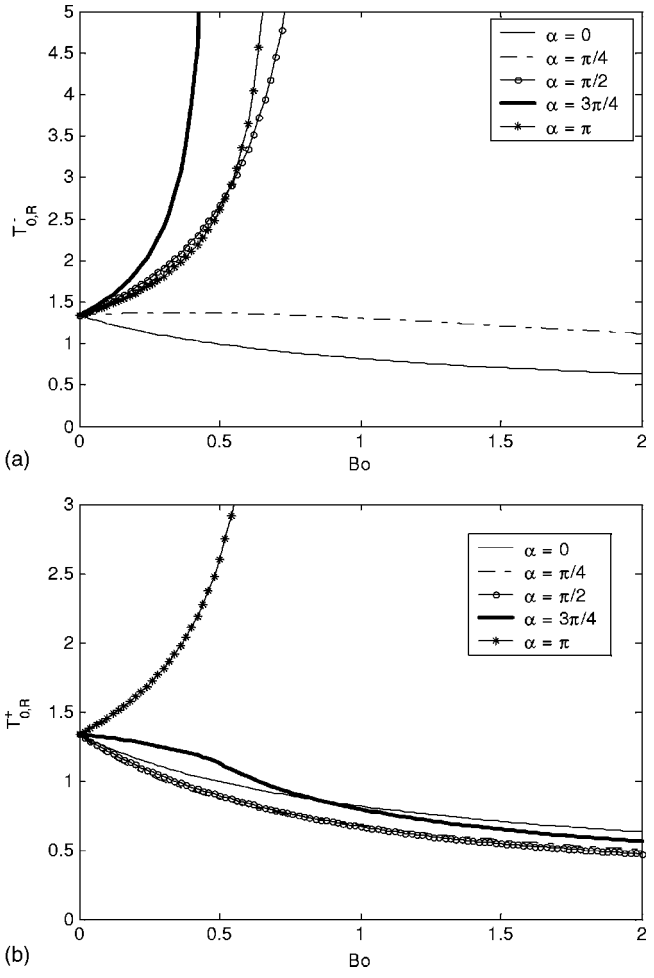

FIG. 4. Trailing film thickness in units of half-channel width vs *Bo* on the (a) lower and (b) upper wall at $O(Ca^0)$.

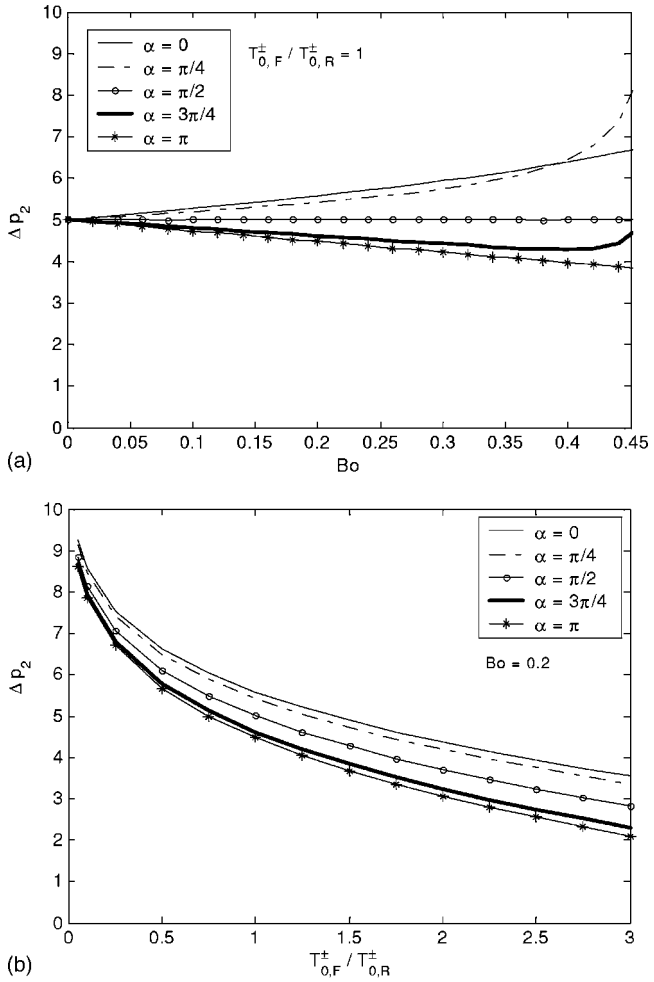

FIG. 5. Flow contribution to pressure drop across the plug as a function of (a) *Bo* and (b) precursor film thickness.

In the front of the plug, the precursor film thickness $T^\pm_{0,F}$ is a specified quantity and (27) serves as an equation for $A^\pm_0$. Thus, to solve for the front transition regions, the constant A in (25) is used as a shooting parameter that is iterated until (27) is satisfied for the particular choice of $T^\pm_{0,F}$. If $h^\pm_{0,xx}(x^\pm_{0,R})=0$ for the rear interface for some (Bo_c, α), then $h^\pm_{0,xx}(x^\pm_{0,F})=0$ for the front interface for $(Bo_c, \pi-\alpha)$. Therefore when $\alpha \leqslant \pi/2$ solutions for the front transition region only exist for $Bo < Bo_c$.

C. Higher-order corrections: Statics region

It can be shown that the $O(Ca^{1/3})$ corrections to the interface shape and pressure, $h^\pm_1$ and p_1, are both equal to zero. As a result the coordinate translation in (24) is found from the matching conditions at $O(Ca^{2/3})$ to be

$$X^\pm_0 = -\frac{A^\pm_1}{A^\pm_0} T^\pm_0. \tag{28}$$

Since $h^\pm_1=0$, the normal stress balance at $O(Ca^{2/3})$ in the statics region can be simplified to

$$\pm \frac{h^\pm_{2,x}}{(1+h^{\pm 2}_{0,x})^{3/2}} = \delta p_2 (x - x_t), \tag{29}$$

with boundary conditions

$$h^\pm_2(x^\pm_0) = -\frac{1}{h^\pm_{0,xx}(x^\pm_0)} \left(\frac{(A^\pm_1)^2}{2} - A^\pm_0 A^\pm_2 \right), \tag{30}$$

obtained by comparing terms independent of X at $O(Ca^{2/3})$ in (17). As before, (29) and (30) are transformed to arc-length coordinates and integrated numerically to determine δp_2. Details can be found in the Appendix.

The pressure drop across the plug is

$$\begin{aligned} \Delta_p &= p_{air,R} - p_{air,F} \\ &= (\delta p_{0,R} + Ca^{2/3} \delta p_{2,R}) - (\delta p_{0,F} + Ca^{2/3} \delta p_{2,F}) + O(Ca) \\ &= \Delta p_0 + Ca^{2/3} \Delta p_2 + O(Ca), \end{aligned} \tag{31}$$

where Δp_0 is the hydrostatic contribution and Δp_2 is the leading-order flow contribution. Since we are primarily interested in the effects of flow, we examine how Δp_2 depends on the system parameters. In Fig. 5(a) Δp_2 is plotted against *Bo* for different α with the precursor film thickness on the lower and upper walls equal to the corresponding trailing film thickness. This corresponds to steady plug propagation in

which the plug volume does not change. For $\alpha<\pi/2$ the pressure drop increases with *Bo*. This is a result of greater viscous stresses associated with the decreasing film thickness at these orientations (see Fig. 3). When $\alpha=\pi/2$ the thickening of the lower film exactly counteracts the thinning of the upper and the pressure drop remains constant. For $\alpha>\pi/2$ the pressure drop initially decreases with *Bo*, but eventually increases and diverges as the film thickness diverges. Figure 5(b) shows that at any orientation Δp_2 decreases as the precursor film thickness increases. This is consistent with previous results[32,34] that showed that it is easier to drive a plug through a tube with thicker precursor film.

D. Higher-order corrections: Transition regions

In the transition regions lubrication equations still apply at $O(Ca^{1/3})$ and the following third-order equation is found for the correction term $H_1^{\pm}(X)$:

$$H_{1,XXX}^{\pm}=-\frac{3(2H_0^{\pm}-3T_0^{\pm})H_1^{\pm}+3T_1^{\pm}H_0^{\pm}+Bo\cos(\alpha)H_0^{\pm}(H_0^{\pm^3}-T_0^{\pm^3})}{H_0^{\pm^4}}. \tag{32}$$

Note that there is a contribution from the gravitational component of the pressure gradient in the x direction, $Bo\cos(\alpha)$. The expression found by Wilson[41] for the dragout problem reduces to (32) after some simplification. The result of Park and Homsy[21] is recovered when $Bo=0$ or $\alpha=\pi/2$. Equation (32) is rescaled as in (24) with $J_1^{\pm}=H_1^{\pm}/T_0^{\pm}$, $\hat{T}_1^{\pm}=T_1^{\pm}/T_0^{\pm}$, $\xi=(X+X_0^{\pm})/T_0^{\pm}$ to get

$$J_{1,\xi\xi\xi}^{\pm}=-\frac{3(2J_0^{\pm}-3)J_1^{\pm}+3\hat{T}_1^{\pm}J_1^{\pm}+Bo\cos(\alpha)T_0^{\pm^2}J_0^{\pm}(J_0^{\pm^3}-1)}{J_0^{\pm^3}}. \tag{33}$$

Initial conditions for integrating (33) are obtained from the asymptotic behavior in the vicinity of the thin films,

$$\begin{aligned} &J_1^{\pm}\sim\hat{T}_{1,R}^{\pm}+A\exp(\lambda\xi),\quad \xi\to-\infty(\text{rear}),\\ &J_1^{\pm}\sim\hat{T}_{1,F}^{\pm}+\exp(-\lambda\xi/2)(A\cos(\sqrt{3}\lambda\xi/2)\\ &\qquad +B\sin(\sqrt{3}\lambda\xi/2)),\quad \xi\to\infty(\text{front}), \end{aligned} \tag{34}$$

where $\lambda=3^{1/3}$ as before. Note that $\hat{T}_{1,R}^{\pm}$ is unknown in the rear, but $\hat{T}_{1,F}^{\pm}$ is specified in the front. Thus the initial conditions involve two unknown constants, ($\hat{T}_{1,R}^{\pm}$, A) in the rear and (A, B) in the front, which are determined by matching the transition region and statics region solutions. In the vicinity of the statics region $J_1^{\pm}$ has the asymptotic form

$$\begin{aligned} &J_1^{\pm}\sim-(Bo\cos(\alpha)(T_0^{\pm})^2/6)\xi^3+(B_0^{\pm}/2)\xi^2+B_1^{\pm}\xi+B_2^{\pm},\\ &\xi\to\pm\infty. \end{aligned} \tag{35}$$

Comparing terms involving X^3, X^2, and X in the $O(Ca)$ matching condition we find

$$h_{0,xxx}^{\pm}(x_0^{\pm})=\pm Bo\cos(\alpha), \tag{36}$$

$$h_{1,xx}^{\pm}(x_0^{\pm})=\left(\frac{B_0^{\pm}}{2T_0^{\pm}}-\frac{Bo\cos(\alpha)X_0^{\pm}}{2}\right), \tag{37}$$

$$h_{2,x}^{\pm}(x_0^{\pm})=\mp\left(B_1^{\pm}+\frac{B_0^{\pm}X_0^{\pm}}{T_0^{\pm}}-\frac{Bo\cos(\alpha)X_0^{\pm^2}}{2}\right). \tag{38}$$

Equation (36) can be obtained from (19) and (21) and provides no new information. Since $h_1^{\pm}$, $h_2^{\pm}$, $T_0^{\pm}$, and $X_0^{\pm}$ are known, (37) and (38) and provide boundary conditions for (33), which is solved by numerical integration using (34) as the initial condition and choosing ($\hat{T}_{1,R}^{\pm}$,A) or (A,B) to satisfy (37) and (38). Figures 6(a) and 6(b) show the $O(Ca)$ correction to the trailing film thickness at the lower and upper walls, $T_{1,R}^{-}$ and $T_{1,R}^{+}$, as a function of *Bo* for different α. When $\alpha<\pi/2$ both $T_{1,R}^{-}$ and T_{1R}^{+} are negative, indicating that this correction makes the film thinner. The opposite is true when $\alpha>\pi/2$. In the former case, $T_{1,R}^{-}$ and $T_{1,R}^{+}$ have slight minima for some orientations, while in the latter $T_{1,R}^{+}$ passes through a maximum for $\alpha=3\pi/4$. Since (33) involves $T_0^{\pm}$ which diverges at $Bo=Bo_c$, $T_{1,R}^{\pm}$ also diverges at Bo_c. When $Bo=0$ or $\alpha=\pi/2$ the gravitational term involving $Bo\cos(\alpha)$ disappears from (33) and the boundary conditions, (37) and (38). As a result $T_{1,R}^{\pm}=0$, which is consistent with the results of Park and Homsy.[21]

IV. THE GRAVITATIONAL REGIME

The analysis in Sec. III breaks down when the curvature of the static solution at the lower wall becomes zero and the film thickness diverges. This occurs when $\alpha\geqslant\pi/2$ for the rear meniscus and $\alpha\leqslant\pi/2$ for the front meniscus. In this section we determine the critical Bond number Bo_c for breakdown and examine the structure of the solution in the lower transition region where this occurs. This analysis applies to either the rear or front interface for appropriate values of α, while the viscocapillary analysis applies to the other interface.

A. Critical Bond number

Since the curvature in the lower transition region becomes small at $Bo=Bo_c$, the gravitational scaling (14) applies in this region while the viscocapillary scaling (11) applies in the upper transition region. The perturbation

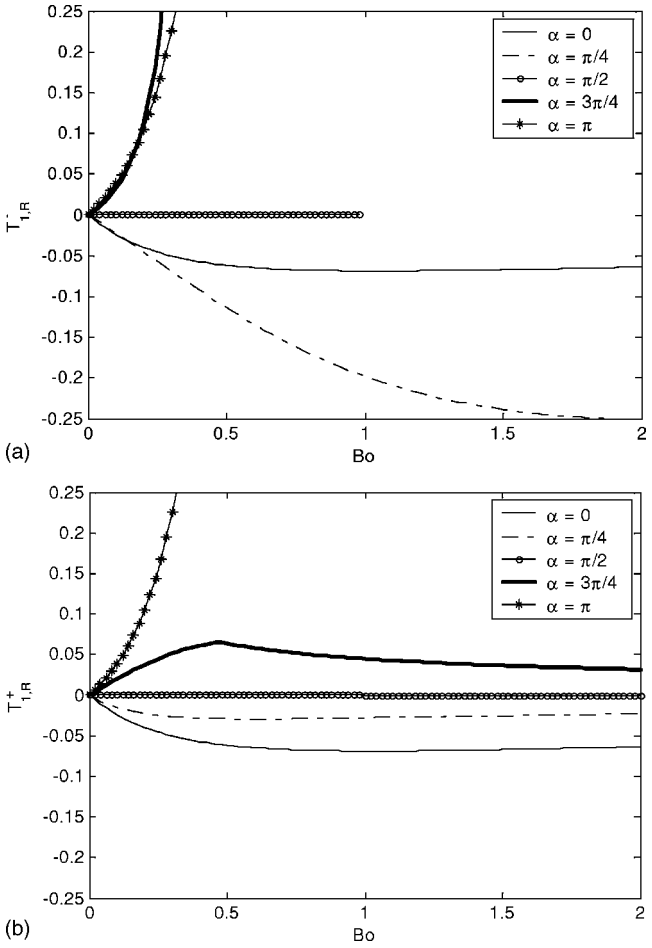

FIG. 6. Trailing film thickness in units of half-channel width vs *Bo* on the (a) lower and (b) upper wall at $O(Ca^{1/3})$.

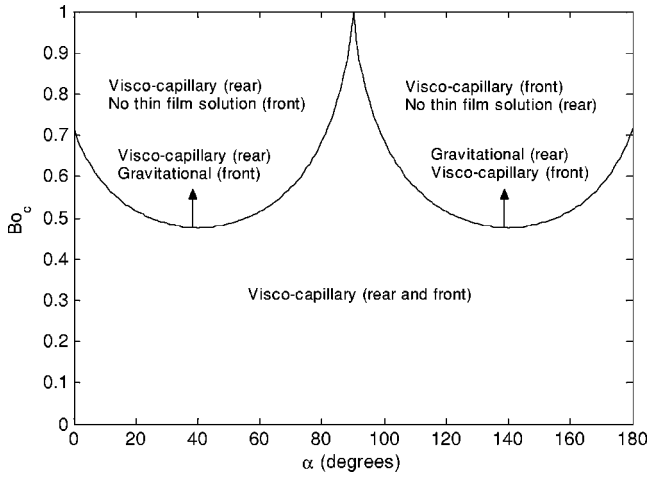

FIG. 7. Critical Bond number Bo_c for different orientations. For $Bo < Bo_c$ the viscocapillary scaling (11) is valid in all transition regions. In the lower transition regions, for $Bo = Bo_c + BCa^{1/6}$ and $\alpha > \pi/2$, the gravitational scaling (14) holds behind the plug and the viscocapillary scaling holds in front of the plug—these scalings are reversed when $\alpha < \pi/2$. The upper transition regions follow the viscocapillary scaling for all *Bo* (except for $\alpha = 0, \pi$ when $Bo \geqslant Bo_c$), however corresponding to $\alpha < \pi/2$ or $\alpha > \pi/2$, this scaling applies either to the rear or the front meniscus, and the opposite meniscus has no thin film solution.

expansion (15) for both regions proceeds in powers of $Ca^{1/6}$. In the statics region, the normal stress condition is identical to (19) at leading order and is reproduced below:

$$Bo_c x \cos(\alpha) - Bo_c h_0^{\pm}(x)\sin(\alpha) - \delta p_0 = \pm \frac{h^{\pm}_{0,xx}}{(1 + h^{\pm 2}_{0,x})^{3/2}}. \tag{39}$$

Boundary conditions are obtained by considering terms involving $h_0^{\pm}(x)$ up to $O(Ca^{1/3})$ in the matching condition (17),

$$O(Ca^0)\text{: } h_0^{\pm}(x_0^{\pm}) = \pm 1, \tag{40}$$

$$O(Ca^{1/6})\text{: } h^-_{0,x}(x_0^-) = 0, \tag{41}$$

$$O(Ca^{1/3})\text{: } h^+_{0,x}(x_0^+) = 0 \tag{42a}$$

$$h^-_{0,xx}(x_0^-) = 0. \tag{42b}$$

Equations (40), (41), and (42a) are identical to (20) and (21), but (42b) is an additional condition that requires the curvature of the statics solution to vanish at the lower wall and provides a constraint to determine Bo_c. The system is transformed to arc-length coordinates as explained in the Appendix and Bo_c is determined as a function of α. Results are plotted in Fig. 7. It is seen that Bo_c has two minima at $\alpha \sim \pi/4$, $3\pi/4$, and a maximum value of 1 at $\alpha = \pi/2$.

B. $O(Ca^0)$ equations in the transition region

The upper transition region is described by (23). Rescaling variables in the lower transition region leads to lubrication equations, which are solved to obtain the following equation for the interface location:

$$J^-_{0,\xi\xi\xi} = \frac{3(J_0^- - 1)}{(J_0^-)^3} - \frac{Bo_c \cos(\alpha)(T_0^-)^2((J_0^-)^3 - 1)}{(J_0^-)^3}, \tag{43}$$

where $J_0^- = H_0^-/T_0^-$, $\xi = (X + X_0^-)/T_0^-$ as in (24). This equation with $\alpha = 0$ was obtained by Derjaguin[40] to describe the thickness of the liquid film on a plate withdrawn from a fluid reservoir. In the context of that problem, different approximations have been used to find solutions of (43) that match to the flat fluid interface in the reservoir.[43,44] Here we describe a solution that uses exact matching conditions to connect the film to the plug in the statics region.

In the vicinity of the thin films J_0^- has the asymptotic form

$$J_0^- \sim 1 + A\exp(\lambda\xi), \quad \xi \to \infty(\text{rear/front}), \tag{44}$$

and λ satisfies

$$\lambda^3 - 3(1 - (T_0^-)^2 Bo_c \cos(\alpha)) = 0. \tag{45}$$

For the rear transition region, (43) is valid when $\alpha > \pi/2$. In this case the single real root of (45), $\lambda = \lambda_R = [3(1 - (T_0^-)^2 Bo_c \cos(\alpha))]^{1/3}$, is positive and initial conditions that decay as $\xi \to -\infty$ can be found. The constant A is arbitrarily set equal to 1 because of the translation X_0^-. In contrast to the viscocapillary regime, the unknown film thickness T_0^- explicitly appears in the equation and initial conditions. It is there-

fore treated as a shooting parameter and determined by matching J_0^- to the statics region, where it has the asymptotic form

$$J_0^- \sim -\frac{Bo_c \cos(\alpha)(T_0^-)^2\xi^3}{6} + \frac{A_0^-\xi^2}{2} + A_1^-\xi + A_2^-, \quad \xi \to \pm\infty(\text{rear/front}). \tag{46}$$

Rewriting (46) in terms of X and matching to appropriate terms at $O(Ca^{1/2})$ in the Taylor series expansion of $h^-(x)$ we find

$$h_{0,xxx}^-(x_0^-) = \pm Bo_c \cos(\alpha), \tag{47}$$

$$h_{1,xx}^-(x_0^-) = \left(\frac{A_0^-}{T_0^-} - Bo_c \cos(\alpha)X_0^-\right), \tag{48}$$

$$h_{2,x}^-(x_0^-) = \left(A_1 + \frac{A_0X_0^-}{T_0^-} - \frac{Bo_c \cos(\alpha)X_0^{-2}}{2}\right). \tag{49}$$

Equation (47) follows from (39) and (41) and does not provide new information. Thus higher-order corrections in the statics region, $h_1^-(x)$ and $h_2^-(x)$, are required to complete the transition region solution. It can be shown that $h_1^\pm(x)$ and $h_2^\pm(x)$ satisfy homogeneous equations and boundary conditions and are equal to zero. Then (48) and (49) provide conditions to determine T_0^- and X_0^- and complete the solution for J_0^-. Figure 8(a) shows T_0^- as a function of α when $Bo=Bo_c$. Note that (43) reduces to the Landau–Levich equation, (23), when $\alpha=\pi/2$ and (48) indicates that T_0^- diverges unless $A_0^-=0$. It was not possible to find a solution with $A_0^-=0$ for $\alpha=\pi/2$. This case has been treated by Jensen *et al.*[35] and we will discuss their results later in this section.

In the front transition region, (43) applies for $\alpha<\pi/2$. If $(T_{0,F}^-)^2 Bo_c \cos(\alpha)<1$, (45) has two roots with negative real part, $\lambda=\lambda_R(-1\pm i\sqrt{3})/2$, which provide decaying solutions as $\xi\to+\infty$ and a solution for J_0^- can be found for each choice of $T_{0,F}^-$. On the other hand, if $(T_{0,F}^-)^2 Bo_c \cos(\alpha)>1$ there is a single root with negative real part, $\lambda=\lambda_R$. Treating $T_{0,F}^-$ as an unknown quantity the procedure used for the rear transition region was followed; however no solutions satisfying (48) and (49) could be found. Thus there is an upper limit to the precursor film thickness for which solutions of the front transition region exist, and within this limit $T_{0,F}^-$ can be chosen arbitrarily.

C. Higher-order corrections: Statics region

Since $h_1^\pm(x)=h_2^\pm(x)=0$, the normal stress balance in the statics region at $O(Ca^{1/2})$ can be simplified to

$$\pm\frac{h_{3,x}^\pm}{(1+h_{0,x}^{-2})^{3/2}} = \delta p_3(x-x_t). \tag{50}$$

Matching terms independent of X at $O(Ca^{1/2})$ in (17) yields

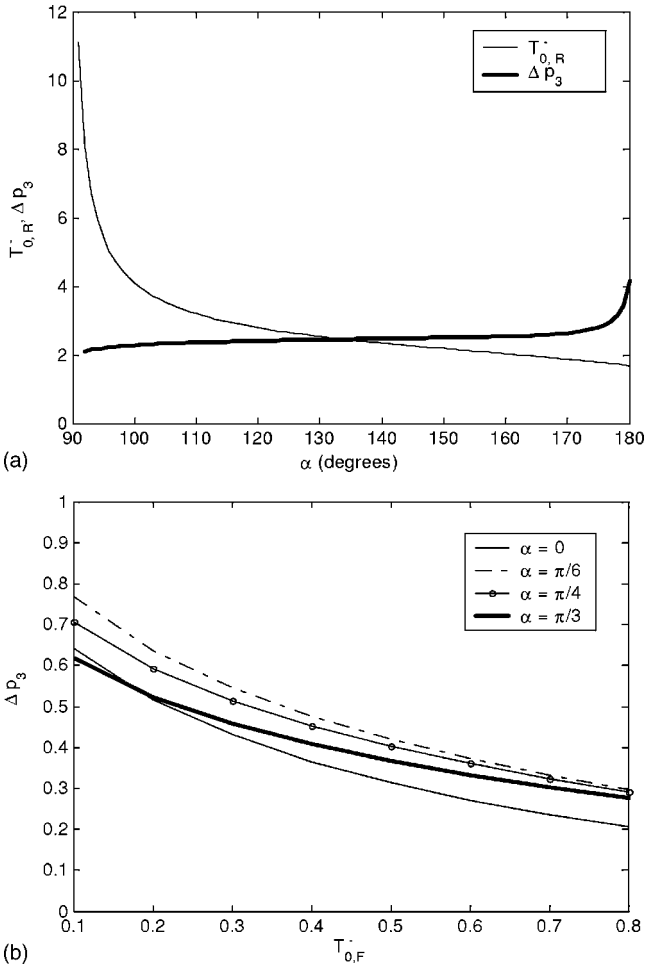

FIG. 8. (a) Trailing film thickness and flow contribution to pressure drop across rear meniscus at $Bo=Bo_c$ and (b) flow contribution to pressure drop across front meniscus as a function of precursor film thickness at $Bo=Bo_c$.

$$h_3^-(x_0^-) = \mp\left(A_2T_0^- + A_1X_0^- + \frac{A_0(X_0^-)^2}{2T_0^-} - \frac{Bo_c \cos(\alpha)(X_0^-)^3}{6}\right), \tag{51}$$

where all the quantities on the right side are known. At the upper wall matching conditions of the viscocapillary regime apply and lead to the homogeneous condition

$$h_3^+(x_0^+) = 0. \tag{52}$$

Equations (51) and (52) specify boundary conditions for $h_3^+(x)$ and $h_3^-(x)$ and the requirement that they join smoothly at $x=x_t$ determines δp_3. When $\alpha=0$ or π, the symmetry condition $h_3^-(x_t)=0$ is used along with either (51) (for the rear interface when $\alpha=\pi$; front interface when $\alpha=0$) or (52) (for the rear interface when $\alpha=0$; front interface when $\alpha=\pi$). The flow contribution to the pressure drop across the plug is dominated by the $O(Ca^{1/2})$ contribution from either the rear or front meniscus, since the drop across the other meniscus is $O(Ca^{2/3})$. δp_3 for the rear meniscus is plotted in Fig. 8(a) versus α and increases with α as the film becomes thinner.

For $\alpha < \pi/2$, Fig. 8(b) shows δp_3 across the front meniscus as a function of $T^-_{0,F}$. As before δp_3 decreases with increasing $T^-_{0,F}$.

It remains to discuss the structure of the solution for $Bo > Bo_c$. For small increments over Bo_c, the Bond number can be expanded in powers of $Ca^{1/6}$, i.e., $Bo = Bo_c + BCa^{1/6}$, $B = O(1) > 0$; and the preceeding approach applies. In this case, the $O(Ca^{1/6})$ and $O(Ca^{1/3})$ statics solutions, $h_1^{\pm}(x)$ and $h_2^{\pm}(x)$, will be nonzero and modify the matching conditions that determine the film thickness. The flow contribution to the pressure drop will be $O(Ca^{1/6})$ while the film thickness remains $O(Ca^{1/2})$. We do not present such an analysis here, but only note that a consistent asymptotic solution can be found.

For higher *Bo*, when the system (39)–(42) was solved by relaxing (40), the interface did not contact the lower wall, but passed through an inflection point at $h_0^-(x_0^-) = y_1$, $-1 < y_1 < 1$. The origin of the transition region is thus located at a distance $(1+y_1)$ above the lower wall and the film thickness is $O(1)$. However, a consistent solution cannot be found because the viscous and body force terms do not balance each other in the *x* momentum equation in the lower film,

$$Ca\frac{\partial^2 u}{\partial y^2} + Bo\cos(\alpha) = 0, \tag{53}$$

if the film thickness is $O(1)$ and $Ca \ll 1$. This inconsistency is the result of neglecting the viscous terms in the normal stress condition that are comparable in size to the other terms in the vicinity of the inflection point. Thus it is necessary to solve for the velocity field and the asymptotic approach breaks down. An exception is the special case $\alpha = \pi/2$ for which the gravitational term vanishes in (53). For $Bo \geqslant Bo_c$, it can be shown that all derivatives of $h_0^-(x)$ vanish at $y = y_1$, the transition region vanishes and the static interface joins smoothly to a film of thickness $(1+y_1)$ that is independent of the capillary number.[35]

V. DISCUSSION

To discuss the application of these results to human airways, we examine the effect of gravity and propagation speed on two features of physiological significance, namely, prebifurcation asymmetry in the liquid distribution and plug rupture. We estimate values for the dimensionless parameters for two cases based on physical properties and airway dimensions and speeds from Cassidy *et al.*[18] and King *et al.*:[47] (1) SRT using the surfactant Survanta [$\rho = 1.16$ g/cm^3, $\mu = 0.52$ g/(cm s), and $\sigma = 48$ dyn/cm] and (2) PLV using perflurorcarbon liquids [$\rho = 1.93$ g/cm^3, $\mu = 0.021$ g/(cm s), and $\sigma = 18$ dyn/cm]. Under these conditions Bond and capillary numbers vary in the range $0.01 < Bo < 0.2$, $0.01 < Ca < 0.1$ (SRT); $0.04 < Bo < 0.6$, $0.001 < Ca < 0.01$ (PLV) between generations 11 and 17 of the adult human lung. In the discussion to follow we use the results of the viscocapillary regime over the parameter range $0.0 < Bo < 0.4$, $0.0 < Ca < 0.05$ which is relevant to SRT and PLV in small airways.

A. Prebifurcation asymmetry

A composite solution for the shape of the interface accurate to $O(Ca^{2/3})$ was obtained by using the method of additive composition,[48]

$$h_c = h_0^{\pm}(x) + Ca^{2/3}h_2^{\pm}(x) \pm \left[1 - Ca^{2/3}(H_0^{\pm}(X) + Ca^{1/3}H_1^{\pm}(X))\right] - c.p., \tag{54}$$

where the common part *c.p.* was determined from the matching conditions to be

$$c.p. = h_0^{\pm}(x_0^{\pm}) + h_{0,xx}^{\pm}(x_0^{\pm})\frac{(x-x_0^{\pm})^2}{2} + h_{0,xxx}^{\pm}(x_0^{\pm})\frac{(x-x_0^{\pm})^3}{6} + Ca^{2/3}\left[h_2^{\pm}(x_0^{\pm}) + h_{2,x}^{\pm}(x_0^{\pm})(x-x_0^{\pm})\right]. \tag{55}$$

Sample interface shapes for different parameter values are graphed in Fig. 9. In this figure and the results to follow, the precursor film thickness on either wall, $h_{\infty,F}^{\pm}$, is fixed at 0.1. In each panel the interface for $Bo = 0$, which is symmetric about the centerline of the channel ($y = 0$), is shown for comparison. When $Bo > 0$, the interface is distorted as more liquid pools below the centerline ($y < 0$). The asymmetry increases with increasing *Ca* and depends on α: The shape of the rear interface is most sensitive to changes in *Bo* and *Ca* for $\alpha > \pi/2$, while the front interface is most sensitive for $\alpha < \pi/2$. Since the precursor film thickness is independent of *Bo* and *Ca*, the shape of the front interface does not vary as much as that of the rear.

An interesting feature of the interface shape is the "necking in" seen at the front meniscus. The nonmonotonic shape represents a capillary wave at the interface and is a result of the oscillatory initial conditions (25) and (34) required for the solution of (23) and (33), respectively. Such profiles have been described by other authors for the motion of long bubbles[20] and plugs in tubes.[32,34] The capillary wave causes the minimum distance between the interface and the channel wall, h_{min}, to be less than the constant film thickness far from the plug. The dependence of h_{min} on *Bo* and α mirrors the variation of the trailing film thickness with these parameters: on the lower wall, h_{min} passes through a slight maximum as *Bo* is increased for $\alpha = \pi/4$, whereas it decreases monotonically with *Bo* for $\alpha = \pi/2$, $3\pi/4$. On the upper wall, h_{min} decreases monotonically with *Bo* for $\alpha = \pi/4$, $\pi/2$, $3\pi/4$.

When the plug splits at an airway bifurcation, the asymmetric liquid distribution can play a role in determining the volume of liquid delivered to each downstream branch (see Fig. 1). In order to quantify the prebifurcation asymmetry, a *volume ratio* V_R is defined as the ratio of the liquid volume above the centerline of the channel to that below per unit width of the channel and is equal to

$$V_R = \frac{V^+ + L_P}{V^- + L_P}, \tag{56}$$

where L_P is the plug length and

$$V^+ = \int_{x_{1,R}^+}^{x_{2,R}} h_{c,R}(x)dx + \int_{x_{2,F}}^{x_{1,F}^+} h_{c,F}(x)dx + (x_t - x_{2,R}) + (x_{2,F} - x_t),$$

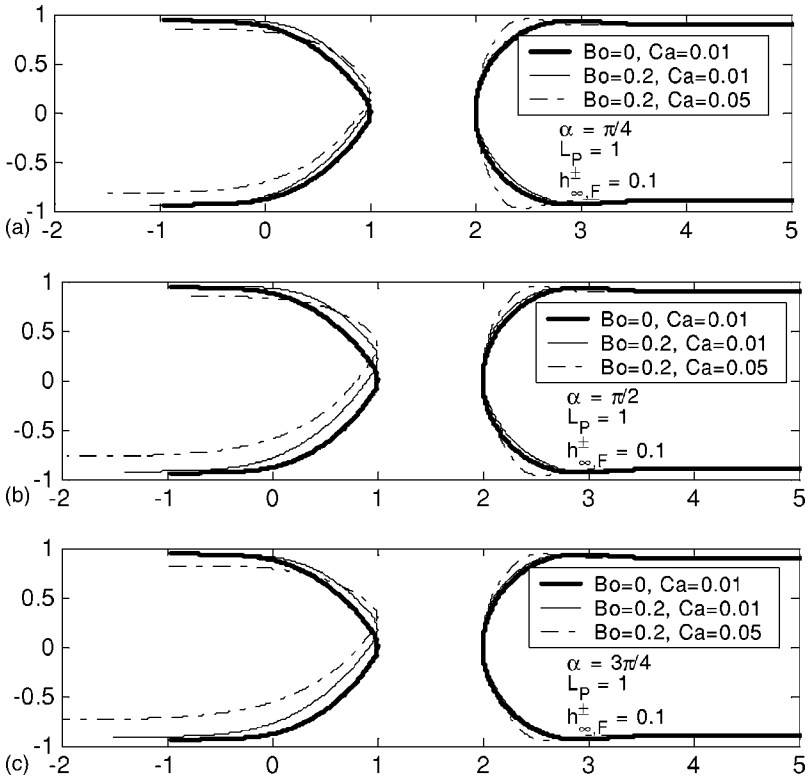

FIG. 9. Composite solution showing the shape of the plug for three combinations of *Bo* and *Ca* at (a) $\alpha=\pi/4$, (b) $\alpha=\pi/2$, and (c) $\alpha=3\pi/4$. Other parameter values are fixed at $h^{\pm}_{\infty,F}=0.1$, $L_p=1$. The interface for $Bo=0$ (dotted line) in each panel is symmetric about $y=0$, but becomes distorted as *Bo* and *Ca* increase.

$$V^{-} = -\int_{x_{1,R}^{-}}^{x_{2,R}} h_{c,R}(x)dx - \int_{x_{2,F}}^{x_{1,F}^{-}} h_{c,F}(x)dx + (x_t - x_{2,R}) + (x_{2,F} - x_t). \tag{57}$$

In (57), $x_{2,R/F}$ and x_t are the locations corresponding to the centerline ($y=h_c=0$) and "tip" ($dh_c/dx\to\infty$), respectively. The other limits of integration, $x^{\pm}_{1,R/F}$, are chosen to be the locations at which the distance between the wall and the interface reaches within 1% of the constant film thickness.

Figures 10 and 11 show the dependence of V_R on different parameters. In Fig. 10(a), V_R is plotted as a function of *Bo* for different orientations with $Ca=0.01$, $L_p=1$. When $Bo=0$, the plug is symmetric about $y=0$, and $V_R=1$, indicating symmetric liquid distribution on either side of the centerline. As *Bo* increases, a progressively larger fraction of the plug volume resides in the lower half of the channel ($y<0$) and V_R decreases. The *Bo* dependence strongly depends on the orientation α, and for $\alpha\geqslant\pi/2$, V_R decreases rapidly, leading to crossovers between the different curves.

Figure 10(b) shows that V_R depends strongly on *Ca* and decreases as *Ca* is increased. The decrease is more pronounced at higher *Bo*. When $Ca=0$, the channel walls are dry and V_R is calculated from the static solution. V_R is less than 1 due to gravitational distortion of the static interface, and this effect increases with *Bo* When $Ca>0$, dynamic effects enhance the gravitational distortion of the interface as seen in Fig. 9 and lead to a decrease in V_R. These results indicate that at low *Ca* in small airways higher propagation speeds lead to more asymmetric plug shapes. When such plugs split at airway bifurcations, the greater liquid volume below the centerline may enhance the amount of liquid delivered to the gravity-preferred branch and thus lead to more nonhomoge-

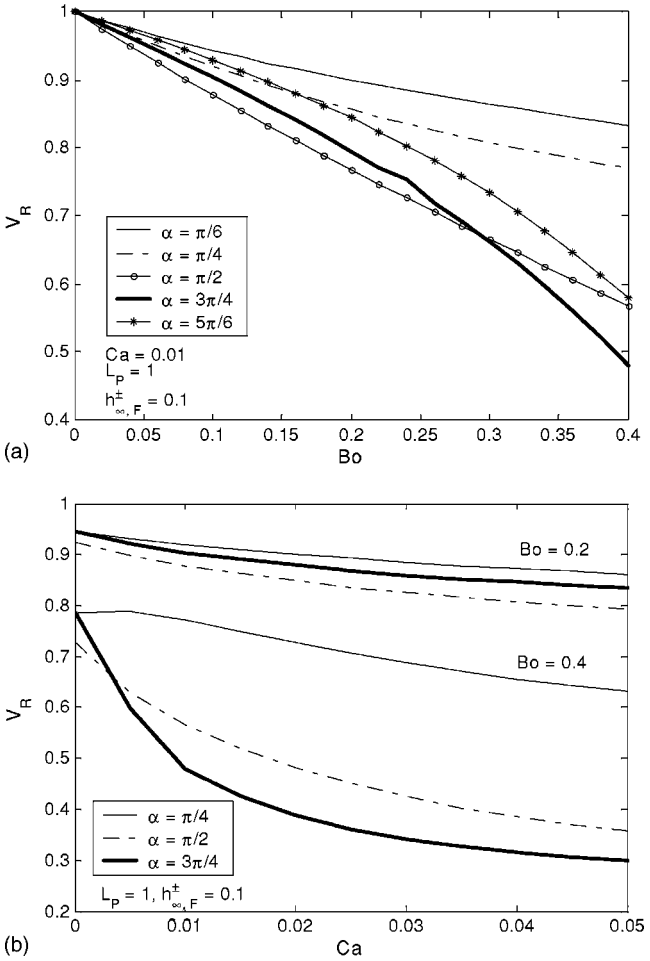

FIG. 10. Ratio, V_R, of liquid volumes per unit channel width above and below centerline, as a function of (a) *Bo* and (b) *Ca* for $L_p=1$ and different values of α.

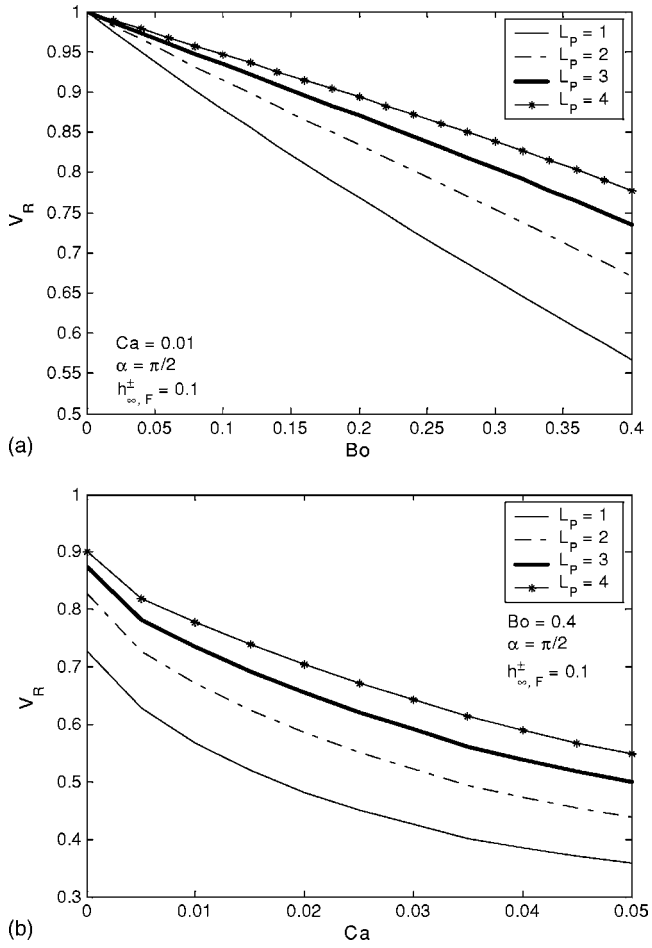

FIG. 11. Ratio, V_R, of liquid volumes per unit channel width above and below centerline, as a function of (a) *Bo* and (b) *Ca* for $\alpha=\pi/2$ and different values of L_p.

neous liquid distribution. This is in contrast to the expected effect of flow in large airways, in which inertial effects could be important due to higher speeds and larger dimensions. Increasing the flow rate under such conditions would counter gravitational effects, leading to more homogeneous plug splitting if the airway bifurcation is geometrically symmetric.

Finally, we consider the effect of plug length L_p. Equation (56) indicates, and Fig. 11 confirms, that V_R increases with L_p as the liquid volume between the tips of the two interfaces increases. Thus the liquid distribution, and hence plug splitting, is likely to be more uniform for longer plugs. However, it must be noted that the asymptotic analysis is only valid for $L_p=O(1)$ since it neglects the fluid mechanical coupling and viscous pressure drop between the front and rear meniscus. These effects become important for very short and very long plugs, respectively.

B. Plug rupture

As the plug moves through the channel its volume decreases if the trailing film is thicker than the precursor film and it eventually ruptures. The instantaneous rate of volume change of the plug is determined by computing the volume flux in the thin films. The velocity profile in the thin films is parabolic since the *x* momentum equation and boundary conditions reduce to

$$Ca\frac{\partial^2 u}{\partial y^2}+Bo\cos(\alpha)=0,$$

$$u(y=\pm 1)=-1,\quad \frac{\partial u}{\partial y}\left(y=\pm(1-h_{\infty}^{\pm})\right)=0. \tag{58}$$

Then the flow rate per unit width of the channel in the precursor films is computed to be

$$Q_F^{\pm}=\frac{Q_F^{*\pm}}{(\mu/\sigma a)}=-Cah_{\infty,F}^{\pm}+\frac{Bo\cos(\alpha)h_{\infty,F}^{\pm 3}}{3}, \tag{59}$$

where the first term represents the constant speed plug motion and the second gravitational drainage. Using the perturbation results of the previous sections the flow rate in the trailing films is

$$Q_R^{\pm}=-Ca^{5/3}T_{0,R}^{\pm}-Ca^2\left(T_{1,R}^{\pm}-\frac{Bo\cos(\alpha)(T_{0,R}^{\pm})^3}{3}\right)+O(Ca^{7/3}). \tag{60}$$

Then the rate at which the plug volume *V* changes with time is

$$\frac{dV}{dt}=(Q_R^{+}+Q_R^{-})-(Q_F^{+}+Q_F^{-}). \tag{61}$$

Figure 12(a) shows a plot of dV/dt against *Ca* for a given *Bo* and precursor film thickness. When *Ca* is small, the trailing film is thin and the volume flux is dominated by gravitational drainage in the precursor films, which can cause the plug volume to increase ($dV/dt>0$) for $\alpha>\pi/2$ and decrease ($dV/dt<0$) for $\alpha<\pi/2$. As *Ca* increases, two opposing effects come into play: the plug picks up more fluid from the precursor films, but also deposits more liquid as the trailing films become thicker. Therefore, for a fixed value of the precursor film thickness, dV/dt passes through a positive maximum and then becomes negative at a critical capillary number Ca_c beyond which the plug volume always decreases and the plug eventually ruptures. Figure 12(b) shows Ca_c as a function of *Bo* for different values of α and $h_{\infty,F}^{\pm}$. When the trailing films become thinner with increasing *Bo* (see Fig. 4), Ca_c increases, while the opposite is true for orientations at which the trailing films become thicker with increasing *Bo*. Ca_c also increases as $h_{\infty,F}^{\pm}$ increases. Thus plug rupture is promoted by higher propagation speeds and thinner precursor films, and is more likely to occur in airways in which the plug motion is opposed by gravity.

C. Summary

We have shown that gravity and channel orientation can have significant effects on the propagation of a liquid plug through a liquid-lined channel. Two different scaling regimes were identified at low capillary number. In the viscocapillary regime which exists for Bond numbers less than an orientation dependent critical value Bo_c, the trailing film thickness, length of the transition region, and flow contribution to the

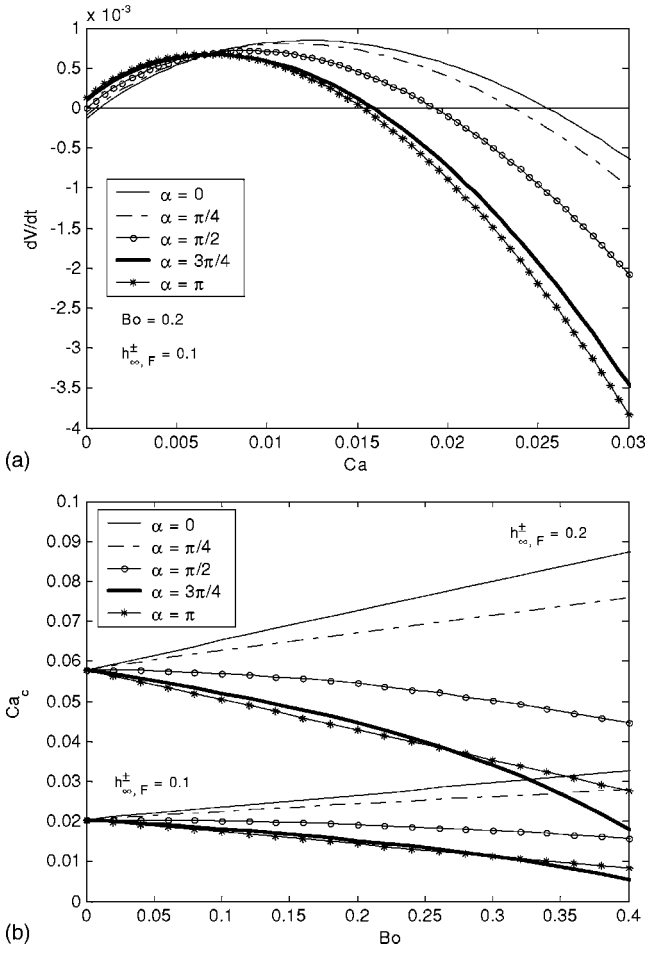

FIG. 12. (a) Rate of change of volume of the plug vs *Ca* and (b) critical capillary number Ca_c vs *Bo* for eventual plug rupture.

pressure drop across the plug scale as $Ca^{2/3}$, $Ca^{1/3}$, and $Ca^{2/3}$, respectively. The first higher-order correction to the film thickness occurs at $O(Ca)$ compared to $O(Ca^{4/3})$ in the no-gravity case. A crossover to the gravitational regime occurs at $Bo=Bo_c$ where these quantities scale as $Ca^{1/2}$, $Ca^{1/6}$, and $Ca^{1/2}$, respectively. For small increments of the Bond number over its critical value ($Bo=Bo_c+Ca^{1/6}B$) the scaling of the film thickness and transition region length remain unchanged, but the pressure drop scales as $Ca^{1/6}$. For higher Bond numbers the small capillary number asymptotics break down and the full Stokes equations must be solved.

The results of the asymptotic analysis were used to examine the effect of gravity on two features of physiological interest, prebifurcation asymmetry in the liquid distribution in the channel and criteria for plug rupture. Asymmetry in the liquid distribution was quantified by calculating the ratio of liquid volumes above and below the centerline of the channel, V_R. V_R depends strongly on α and decreases with *Bo*, but increases with the plug length L_p. An interesting result was that V_R decreases with *Ca*, i.e., the asymmetry in the liquid distribution increases with the plug propagation speed. Thus higher propagation speeds may promote unequal plug splitting at airway bifurcations and increase the inhomogeneity in the overall liquid distribution in the lung. This result is valid in small airways at low speeds when liquid inertia is negligible, and is in contrast to the behavior expected in large airways in which higher speeds would increase inertial effects and result in a more uniform liquid distribution.

Criteria for plug rupture were obtained by determining a critical capillary number Ca_c as a function of *Bo*, α and the precursor film thickness, above which the plug eventually ruptures. Plug rupture limits the depth of penetration of instilled liquid into the lung and thus affects the overall delivery. We found that, in general, plug rupture occurs at lower speeds (lower Ca_c) when the plug motion is opposed by gravity and in channels with thinner precursor films.

These calculations are based on a two-dimensional (2D) channel geometry, whereas a real airway has a cylindrical geometry in which the shape of the interface is not symmetric about the airway axis and the trailing film thickness in a cross-section normal to the axis varies with the azimuthal angle. Analogously, in the 2D channel, gravitational effects distort the interface shape and lead to different film thickness on the upper and lower walls. Many of the interesting results of our study, such as the nonhomogeneous liquid distribution and the (*Bo*, α) dependence of critical capillary number for plug rupture are a result of this gravitationally induced asymmetry and therefore will be present in cylindrical airways as well. While the quantitative dependence of the results on the system parameters will depend on the geometry, the scaling relations in the limit of small *Ca* are identical in either case and therefore the results for the 2D channel will provide insight into the behavior in the cylindrical geometry as well.

The asymptotic analysis presented here provides insight into the physical processes influencing the low capillary number dynamics of plugs in small airways with plug lengths comparable to the airway radius, and does not address the transport of instilled liquid from large airways to smaller ones. This initial transport process is important since it determines input parameters to the current model such as the plug length, which affects liquid distribution and plug rupture. Since inertial effects become important at the length and velocity scales prevalent in large airways, the equations of motion need to be solved numerically. Recent studies have examined finite Reynolds number effects in gravity-free Bretherton type problems propagation using scaling arguments[49,50] and numerical computations.[51–54] These studies, in general, have found that inertial effects lead to a slight decrease in the trailing film thickness at Reynolds numbers less than about 100; however, there is a large increase in the driving pressure and significant changes in the flow and pressure fields in the liquid.[53,54]

ACKNOWLEDGMENTS

This work was supported by NIH Grants No. HL41126, No. HL64373, NSF Grant No. BES-9820967, and NASA Grant No. NAG3-2196.

APPENDIX

An arc-length coordinate system $(s,\theta(s))$ is defined where s is the arc length along the air-liquid interface. The origin is located at the contact point of the static interface

with the upper wall. The interface transforms as $(x, h^{\pm}(x)) \mapsto (\zeta(s), \eta(s))$ with

$$\frac{d\zeta}{ds} = \begin{cases} \cos(\theta) & \text{(rear)} \\ -\cos(\theta) & \text{(front)}, \end{cases} \tag{A1}$$

$$\frac{d\eta}{ds} = -\sin(\theta). \tag{A2}$$

The curvature is given by $\pm h^{\pm}_{xx}/(1+h_x^{\pm 2})^{3/2} = -d\theta/ds$ and the normal stress balance without the viscous term is

$$\frac{d\theta}{ds} = \delta p - Bo\zeta(s)\cos(\alpha) + Bo\,\eta(s)\sin(\alpha). \tag{A3}$$

$\zeta(s)$, $\eta(s)$, $\theta(s)$, and δp are expanded in the perturbation series (15) to obtain equations in the statics region at each order.

1. Equations at $O(Ca^0)$

The equations at leading order are identical in the viscocapillary and gravitational regimes,

$$\frac{d\zeta_0}{ds} = \begin{cases} \cos(\theta_0(s)) & \text{(rear)} \\ -\cos(\theta_0(s)) & \text{(front)}, \end{cases} \tag{A4}$$

$$\frac{d\eta_0}{ds} = \sin(\theta_0(s)), \tag{A5}$$

$$\frac{d\theta_0}{ds} = \Delta p_0 - Bo\zeta_0(s)\cos(\alpha) + Bo\,\eta_0(s)\sin(\alpha). \tag{A6}$$

Boundary conditions (20), (21), (40), (41), and (42a) become

$$\zeta_0 = 0, L_P;\ \eta_0 = 1;\ \theta_0 = 0, \quad s = 0,$$

$$\eta_0 = -1;\ \theta_0 = \pi, \quad s = s_\pi, \tag{A7}$$

which provide three conditions to integrate (A4)–(A6) and two more to determine Δp_0 and s_π. The smoothness condition (22) implies that

$$\theta_0 = \pi/2, \quad \theta_i = 0 (i > 0), \quad \zeta_0 = x_t, \quad s = s_{\pi/2}. \tag{A8}$$

The condition (42b) used to determine Bo_c in the gravitational regime becomes

$$\frac{d\theta_0}{ds} = 0,\ s = s_\pi. \tag{A9}$$

2. Equations at $O(Ca^{1/2})$ and $O(Ca^{2/3})$

The first nonzero corrections to the statics region are $(\zeta_2(s), \eta_2(s), \theta_2(s), \delta p_2)$ at $O(Ca^{2/3})$ in the viscocapillary regime and $(\zeta_3(s), \eta_3(s), \theta_3(s), \delta p_3)$ at $O(Ca^{1/2})$ in the gravitational regime, which satisfy the same equations

$$\frac{d\zeta_{2/3}}{ds} = \begin{cases} -\sin(\theta_0)\theta_{2/3} & \text{(rear)} \\ \sin(\theta_0)\theta_{2/3} & \text{(front)}, \end{cases} \tag{A10}$$

$$\frac{d\eta_{2/3}}{ds} = -\cos(\theta_0)\theta_{2/3}, \tag{A11}$$

$$\frac{d\theta_{2/3}}{ds} = \Delta p_{2/3} - Bo\zeta_{2/3}\cos(\alpha) + Bo\,\eta_{2/3}\sin(\alpha). \tag{A12}$$

The boundary conditions follow from (22), (30) and (51), (52):

$$\left.\begin{aligned} &\zeta_{2/3} = 0 \\ &\eta_2 = -(A_0^+ X_0^{+2}/2T_0^+ + A_1^+ X_0^+ + A_2^+ T_0^+) \\ &\eta_3 = 0 \end{aligned}\right\}, \quad s = 0,$$

$$\left.\begin{aligned} &\zeta_{2/3} = 0 \\ &\eta_2 = (A_0^- X_0^{-2}/2T_0^- + A_1^- X_0^- + A_2^- T_0^-) \\ &\eta_3 = \left(-\frac{Bo_c\cos(\alpha)X_0^{-3}}{6} + \frac{A_0^- X_0^{-2}}{2T_0^-} + A_1^- X_0^- + A_2^- T_0^-\right) \end{aligned}\right\}, \quad s = s_\pi. \tag{A13}$$

When $\alpha = 0$ or π, solutions are symmetric about $y = 0$, i.e., $s = s_{\pi/2}$. The domain of integration is $(s_{\pi/2}, s_\pi)$ and the conditions at $s = 0$ are replaced by

$$\eta_{2/3} = 0, \quad s = s_{\pi/2},$$

$$\zeta_{2/3} = 0, \quad s = s_\pi. \tag{A14}$$

[1] L. K. Hastings, W. H. Renfro, and R. Sharma, "Comparison of beractant and calfactant in a neonatal intensive care unit," Am. J. Health Syst. Pharm. **61**, 257 (2004).
[2] A. H. Jobe, "Pulmonary surfactant therapy," N. Engl. J. Med. **328**, 861 (1993).
[3] H. Yapicioglu, D. Yildizdas, I. Bayram, Y. Sertdemir, and H. L. Yilmaz, "The use of surfactant in children with acute respiratory distress syndrome: Efficacy in terms of oxygenation, ventilation, and mortality," Pulm. Pharmacol. Ther. **16**, 327 (2003).
[4] B. P. Fuhrman, P. R. Paczan, and M. DeFrancisis, "Perfluorocarbon-

associated gas exchange," Crit. Care Med. **19**, 712 (1991).
[5]R. B. Hirschl, M. Croce, D. Gore, H. Wiedemann, K. Davis, J. Zwischenberger, and R. H. Bartlett, "Prospective, randomized, controlled pilot study of partial liquid ventilation in adult acute respiratory distress syndrome," Am. J. Respir. Crit. Care Med. **165**, 781 (2002).
[6]P. N. Cox, H. Frndova, O. Karlsson, S. Holowka, and C. A. Bryan, "Fluorocarbons facilitate lung recruitment," Intensive Care Med. **29**, 2297 (2003).
[7]K. Mikawa, K. Nishina, Y. Takao, and H. Obara, "Efficacy of partial liquid ventilation in improving acute lung injury induced by intratracheal acidified infant formula: Determination of optimal dose and positive end-expiratory pressure level," Crit. Care Med. **32**, 209 (2004).
[8]D. J. Weiss, T. P. Strandjord, J. C. Jackson, J. G. Clark, and D. Liggitt, "Perfluorochemical liquid-enhanced adenoviral vector distribution and expression in lungs of spontaneously breathing rodents," Exp. Lung Res. **25**, 317 (1999).
[9]D. J. Smith, L. M. Gambone, T. Tarara, D. R. Meays, L. A. Dellamary, C. M. Woods, and J. Weers, "Liquid dose pulmonary instillation of gentamicin PulmoSpheres (R) formulations: Tissue distribution and pharmacokinetics in rabbits," Pharm. Res. **18**, 1556 (2001).
[10]J. J. Haitsma, U. Lachmann, and B. Lachmann, "Exogenous surfactant as a drug delivery agent," Adv. Drug Delivery Rev. **47**, 197 (2001).
[11]Y. L. Zhang, O. K. Matar, and R. V. Craster, "A theoretical study of chemical delivery within the lung using exogenous surfactant," Med. Eng. Phys. **25**, 115 (2003).
[12]S. Iqbal, S. Ritson, I. Prince, J. Denyer, and M. L. Everard, "Drug delivery and adherence in young children," Pediatr. Pulmonol **37**, 311, (2004).
[13]P. B. Myrdal, K. L. Karlage, S. W. Stein, B. A. Brown, and A. Haynes, "Optimized dose delivery of the peptide cyclosporine using hydrofluoroalkane-based metered dose inhalers," J. Pharm. Sci. **93**, 1054 (2004).
[14]F. F. Espinosa and R. D. Kamm, "Meniscus formation during tracheal instillation of surfactant," J. Appl. Physiol. **85**, 266 (1998).
[15]K. J. Cassidy, J. L. Bull, M. R. Glucksberg, C. A. Dawson, S. T. Haworth, R. B. Hirschl, N. Gavriely, and J. B. Grotberg, "A rat lung model of instilled liquid transport in the pulmonary airways," J. Appl. Physiol. **90**, 1955 (2001).
[16]J. C. Anderson, R. C. Molthen, C. A. Dawson, S. T. Haworth, J. L. Bull, M. R. Glucksberg, and J. B. Grotberg, "Effect of ventilation rate on instilled surfactant distribution in the pulmonary airways of rats," J. Appl. Physiol. **97**, 45 (2004).
[17]J. L. Bull, S. Tredici, E. Komori, D. O. Brant, J. B. Grotberg, and R. B. Hirschl, "Distribution dynamics of perfluorocarbon delivery to the lungs: An intact rabbit model," J. Appl. Physiol. **96**, 1633 (2004).
[18]K. J. Cassidy, N. Gavriely, and J. B. Grotberg, "Liquid plug flow in straight and bifurcating tubes," J. Biomech. Eng. **123**, 580 (2001).
[19]V. Sauret, R. M. Halson, I. W. Brown, J. S. Fleming, and A. G. Bailey, "Study of the three-dimensional geometry of the central conducting airways in man using computed tomographic (CT) images," J. Anat. **200**, 123 (2002).
[20]F. P. Bretherton, "The motion of long bubbles in tubes," J. Fluid Mech. **10**, 166 (1961).
[21]C.-W. Park and G. M. Homsy, "Two-phase displacement in Hele Shaw cells: theory," J. Fluid Mech. **139**, 291 (1984).
[22]H. Wong, C. J. Radke, and S. Morris, "The motion of long bubbles in polygonal capillaries. Part 1. Thin films," J. Fluid Mech. **292**, 71 (1995).
[23]H. Wong, C. J. Radke, and S. Morris, "The motion of long bubbles in polygonal capillaries. Part 2. Drag, fluid pressure and fluid flow," J. Fluid Mech. **292**, 95 (1995).
[24]L. W. Schwartz, H. M. Princen, and A. D. Kiss, "On the motion of bubbles in capillary tubes," J. Fluid Mech. **172**, 259 (1986).
[25]G. M. Ginley and C. J. Radke, "Influence of soluble surfactants on the flow of long bubbles through a cylindrical capillary," ACS Symp. Ser. **396**, 480 (1988).
[26]J. Ratulowski and H.-C. Chang, "Marangoni effects of trace impurities on the motion of long gas bubbles in capillaries," J. Fluid Mech. **210**, 303 (1990).
[27]C.-W. Park, "Influence of soluble surfactants on the motion of finite bubble in a capillary tube," Phys. Fluids A **4**, 2335 (1992).
[28]K. J. Stebe and D. Bathés-Biesel, "Marangoni effects of adsorption-desorption controlled surfactants on the leading end of an infinitely long bubble in a capillary," J. Fluid Mech. **286**, 25 (1995).
[29]A. Mazouchi and G. M. Homsy, "Thermocapillary migration of long bubbles in cylindrical capillary tubes," Phys. Fluids **12**, 542 (2000).
[30]A. Mazouchi and G. M. Homsy, "Thermocapillary migration of long bubbles in polygonal tubes. I. Theory," Phys. Fluids **13**, 1594 (2001).
[31]D. Halpern and O. E. Jensen, "A semi-infinite bubble advancing into a planar tapered channel," Phys. Fluids **14**, 431 (2002).
[32]P. D. Howell, S. L. Waters, and J. B. Grotberg, "The propagation of a liquid bolus along a liquid-lined flexible tube," J. Fluid Mech. **406**, 309 (2000).
[33]O. E. Jensen, M. K. Horsburgh, D. Halpern, and D. P. Gaver, "The steady propagation of a bubble in a flexible-walled channel: Asymptotic and computational models," Phys. Fluids **14**, 443 (2002).
[34]S. L. Waters and J. B. Grotberg, "The propagation of a surfactant laden liquid plug in a capillary tube," Phys. Fluids **14**, 471 (2002).
[35]M. H. Jensen, A. Libchaber, P. Pelce, and G. Zocchi, "Effect of gravity on the Saffman–Taylor meniscus: Theory and experiment," Phys. Rev. A **35**, 2221 (1987).
[36]D. Lasseux and M. Quintard, "Film thickness behind a receding meniscus," C. R. Acad. Sci., Ser. II: Mec., Phys., Chim., Sci. Terre Univers **313**, 1375 (1991).
[37]D. Lasseux, "Drainage in a capillary—A complete approximated description of the interface," C. R. Acad. Sci., Ser. IIb: Mec., Phys., Chim., Astron. **321**, 125 (1995).
[38]D. Quéré, "Fluid coating on a fiber," Annu. Rev. Fluid Mech. **31**, 347 (1999).
[39]L. D. Landau and V. G. Levich, "Dragging of a liquid by a moving plate," Acta Physicochim. URSS **17**, 42 (1942).
[40]B. V. Derjaguin, "On the thickness of the liquid film adhering to the walls of a vessel after emptying," Acta Physicochim. URSS **20**, 349 (1943).
[41]S. D. R. Wilson, "The drag-out problem in film coating theory," J. Eng. Math. **16**, 209 (1982).
[42]B. V. Derjaguin and S. M. Levi, *Film Coating Theory* (Focal, London, 1964).
[43]A. de Ryck and D. Quere, "Gravity and inertia effects in plate coating," J. Colloid Interface Sci. **203**, 278 (1998).
[44]D. A. White and J. A. Tallmadge, "Theory of drag out of liquids on flat plates," Chem. Eng. Sci. **20**, 33 (1965).
[45]J. R. Cash, G. Moore, and R. W. Wright, "An automatic continuation strategy for the solution of singularly perturbed linear 2-point boundary-value-problems," J. Comput. Phys. **122**, 266 (1995).
[46]J. R. Cash, G. Moore, and R. W. Wright, "An automatic continuation strategy for the solution of singularly perturbed nonlinear boundary value problems," ACM Trans. Math. Softw. **27**, 245 (2001).
[47]D. M. King, Z. D. Wang, H. J. Palmer, B. A. Holm, and R. H. Notter, "Bulk shear viscosities of endogenous and exogenous lung surfactants," Am. J. Physiol. **282**, L277 (2002).
[48]M. Van Dyke, *Perturbation Methods in Fluid Mechanics* (Academic, Boston, 1964).
[49]P. Aussillous and D. Quere, "Quick deposition of a fluid on the wall of a tube," Phys. Fluids **12**, 2367 (2000).
[50]A. de Ryck, "The effect of weak inertia on the emptying of a tube," Phys. Fluids **14**, 2102 (2002).
[51]M. D. Giavedoni and F. A. Saita, "The axisymmetric and plane cases of a gas phase steadily displacing a Newtonian liquid—A simultaneous solution of the governing equations," Phys. Fluids **9**, 2420 (1997).
[52]M. D. Giavedoni and F. A. Saita, "The rear meniscus of a long bubble steadily displacing a Newtonian liquid in a capillary tube," Phys. Fluids **11**, 786 (1999).
[53]M. Heil, "Finite Reynolds number effects in the Bretherton problem," Phys. Fluids **13**, 2517 (2001).
[54]H. Fujioka and J. B. Grotberg, "Steady propagation of a liquid plug in a two-dimensional channel," J. Biomech. Eng. **126**, 567 (2004).